Three-photon polarization entanglement of green light

Yan-Chao Lou (娄严超),[1,2,‡] Zhi-Cheng Ren (任志成)●,[1,2,‡] Chao Chen (陈超),[1,2,*] Pei Wan (万佩),[1,2]
Wen-Zheng Zhu (朱文正),[1,2] Jing Wang (王晶),[1,2] Shu-Tian Xue (薛舒天),[1,2]
Bo-Wen Dong (董博文),[1,2] Jianping Ding (丁剑平)●,[1,2] Xi-Lin Wang (汪喜林),[1,2,3,4,†] and
Hui-Tian Wang (王慧田)●[1,2,5]

[1]*National Laboratory of Solid State Microstructures and School of Physics, Nanjing University,
Nanjing 210093, China*

[2]*Collaborative Innovation Center of Advanced Microstructures, Nanjing University, Nanjing 210093, China*

[3]*Hefei National Laboratory, Hefei 230088, China*

[4]*Synergetic Innovation Center of Quantum Information and Quantum Physics, University of Science and
Technology of China, Hefei 230026, China*

[5]*Collaborative Innovation Center of Extreme Optics, Shanxi University, Taiyuan 030006, China*

Recently, great progress has been made in the entanglement of multiple photons at various wavelengths and with different degrees of freedom for optical quantum information applied in diverse scenarios. However, multiphoton entanglement in the transmission window of green light under water has not yet been reported. Here, by combining femtosecond-laser-based multiphoton entanglement and entanglement-maintaining frequency up-conversion techniques, we successfully generate a green two-photon polarization-entangled Bell state and a green three-photon Greenberger-Horne-Zeilinger state, whose state fidelities are 0.893 ± 0.002 and 0.595 ± 0.023, respectively. Our result provides a scalable method to prepare green multiphoton entanglement, which may have wide applications in underwater quantum information.

I. INTRODUCTION

Multiqubit entanglement is the fundamental quantum resource in quantum physics and quantum information applications [1–5]. The photon, due to its weak interaction with the environment, is the most promising flying qubit, which can carrier quantum information in its various degrees of freedom, such as polarization and optical orbital angular momentum [6–8]. Over the past two decades, multiphoton entanglement has played a crucial role in fundamental quantum physics and quantum information, such as in quantum teleportation [9–12], the test of quantum nonlocality [13–15], and long-distance quantum communication [16–18]. Compared with quantum communication based on mobile devices such as satellites and drones over land [19–21], space-to-water and underwater quantum communication, shown in Fig. 1(a), lags far behind. Because of the absence of underwater entangled photon sources, previous underwater quantum communications have all been implemented with single photons

[22–24]. As is well known, the absorption of light at different wavelengths varies exceedingly in water, as shown in Fig. 1(b) [25,26]. Green light lies in the transmission window of light in water [27], which makes green-photon entanglement essential for underwater and space-to-water quantum communication.

Although spontaneous parametric down-conversion (SPDC) has been widely used to prepare multiphoton entanglement [28–31], including the record 12-photon entanglement at 1560 nm [32], the generation of green multiphoton entanglement states has long been a challenge. Using SPDC from 260 to 520 nm to directly prepare green-photon entanglement faces three problems. The first is that few high-power lasers are available around 260 nm to pump the required SPDC process. Second, appropriate nonlinear crystals are relatively absent, because the known nonlinear crystals such as lithium niobate and potassium titanyl phosphate have generally strong absorption in the ultraviolet and deep-ultraviolet regions [33], and for others such as β-barium borate (β-BBO) and lithium triborate (LBO) it is very difficult to achieve phase matching, although they are transparent in those regimes. Third, commercial optical components that can be used at 260 nm are also scarce.

---

*Contact author: chaochen@nju.edu.cn
†Contact author: xilinwang@nju.edu.cn
‡These authors contributed equally to this work.
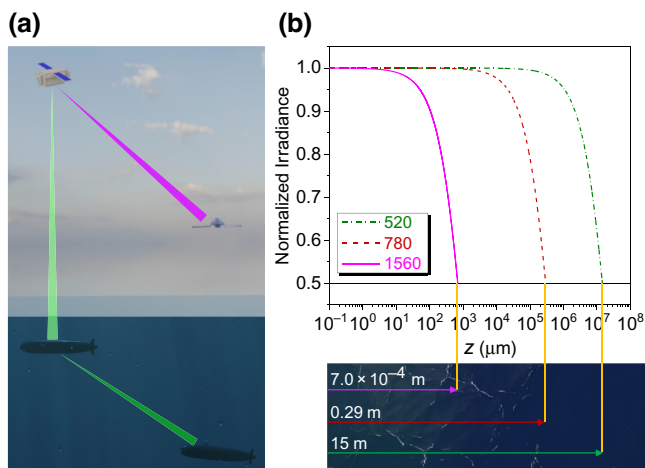
(a)   **(b)**

FIG. 1. (a) Schematic scenarios of space-to-water and multi-party underwater quantum communication. (b) Propagation distance of light at wavelengths of 1560, 780, and 520 nm in water, when the irradiance is reduced to half. Photons at 520 nm have lower absorption and travel farther in water.

The mainstream method for obtaining short-wavelength quantum sources relies on single-photon frequency conversion [34–41], which has shown great potential in connecting platforms working in different wavebands [42–44]. According to the interaction distance between the photons and nonlinear materials, resulting in different conversion efficiencies, defined by the ratio between the converted photon number and the incoming number of signal photons, frequency conversion can be divided into two types with long and short interaction distances. To achieve long interaction distance, one can choose interacting light with long coherence length, including continuous light and picosecond (ps) pulsed laser, which supports nonlinear interaction in a long medium including a waveguide to achieve a high up-conversion efficiency of up to tens of percent [44]. However, in some special application scenarios, for example, to realize spatial structure-preserving frequency conversion, the interaction is restricted near the image plane [45,46] and the corresponding interaction length is limited. In these circumstances, a femtosecond (fs) pulsed laser with a high peak power would be a better choice, although the conversion efficiency is several percent [47,48], about one order lower than that with a picosecond pulsed laser.

So far, the most widely used approach to prepare a multi-photon entanglement source is to connect multiple pairs of entangled two photons [49], which requires high indistinguishability between independent photons from different pairs in the temporal, frequency, and spatial domains. To achieve high indistinguishability in the time domain, pulsed light is employed as pump source. More specifically, it is much easier to realize high indistinguishability with a femtosecond pulse than with a picosecond pulse,

which needs strong filtering. Therefore, the brightness of a multiphoton source based on a femtosecond pulse is much higher than for a picosecond pulse. For example, for a four-photon entanglement source by connecting two pairs of entangled two photons, the brightness with the femtosecond pulse is about five orders higher than for the picosecond pulse [31,32,50–52]. Up to now, the maximum number of entangled photons with a picosecond pulse is four [50], whereas a femtosecond pulse has enabled successful demonstration of up to 12-photon entanglement [32]. Therefore, the femtosecond pulse is more suitable for achieving a short-wavelength multiphoton entanglement source.

Here, we design a protocol to generate three-photon entanglement of green light, by first preparing a multiphoton (including infrared and green photons) polarization-entangled state via femtosecond-laser-pumped SPDC and then exploiting frequency up-conversion to convert the infrared photons to green ones. To realize the frequency conversion of a photon that is polarization-entangled with other photons, we imbed the frequency transducer in a Sagnac interferometer [53,54], where the horizontally and vertically polarized components are both frequency up-converted by passing through the transducer in opposite directions. After outputting from the Sagnac interferometer, orthogonally polarized up-converted photons coherently combine and maintain their polarization entanglement with other photons [55]. Until now, it has remained a challenge to realize femtosecond-pulse-based polarization-entanglement-maintaining frequency up-conversion.

II. EXPERIMENTAL DETAILS

In this paper, we develop a polarization-entanglement-maintaining Sagnac frequency-transducer technology to get 520-nm three-photon entanglement based on SPDC sources as shown in Fig. 2(a). First, a pair of entangled photons at 1560 and 520 nm are generated by SPDC pumped by a femtosecond laser at 390 nm, which is a frequency doubling of the femtosecond laser at 780 nm. Then polarization-entanglement-maintaining frequency up-conversion is implemented to transfer the frequency of the single photon from 1560 nm to 520 nm. The scalability of this scheme pumped by the femtosecond laser is shown by interfering one of the entangled two green photons with another photon pair (at 520 and 1560 nm) to generate three-photon entanglement at 520 nm heralded by a single photon at 1560 nm. Our green three-photon entanglement combines the femtosecond laser pumped SPDC with the frequency up-conversion technique, which provides an innovative way to generate scalable entanglement of green photons, and may pave the way for entanglement-based underwater quantum communication.
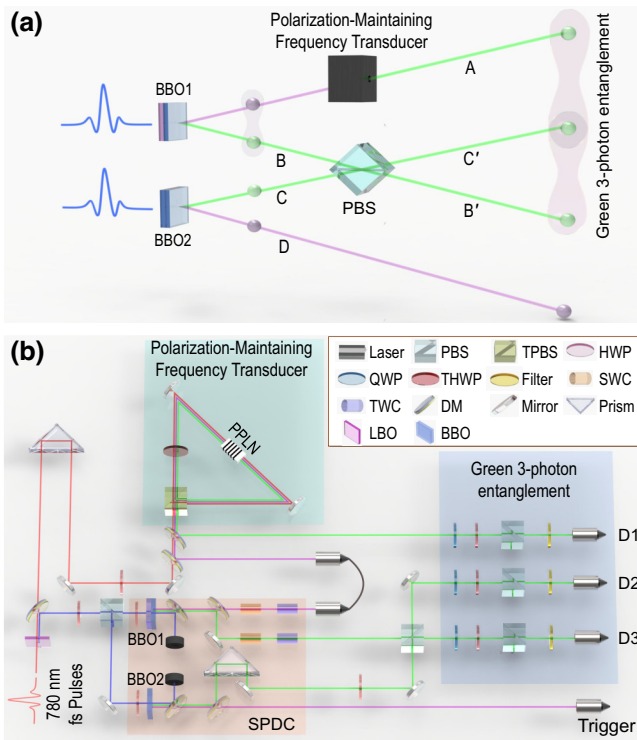
FIG. 2. (a) Schematic diagram for preparing a green three-photon entanglement state. (b) Experimental setup: PBS, polarization beam splitter; TPBS, triple polarization beam splitter; HWP, half-wave plate; QWP, quarter-wave plate; THWP, triple half-wave plate; SWC, space walk-off compensation; TWC, time walk-off compensation; DM, dichroic mirror; PPLN, periodically poled lithium niobate; and D1–D3, detectors. A femtosecond pulsed laser at 780 nm is focused on a frequency-doubling LBO crystal to generate femtosecond laser pulses at 390 nm, which then pump two BBO crystals (BBO1 and BBO2) where pairs of single photons are generated. The PPLN is used for up-converting the single photon at 1560 nm to 520 nm under the pump of another laser at 780 nm. Due to the Sagnac interferometer configuration, the frequency up-conversion is polarization-independent, with the coherence in the polarization state being preserved. The TPBS and THWP in the Sagnac interferometer function at three wavelengths of 1560, 780, and 520 nm. The three green photons are finally detected by D1, D2, and D3, heralded by a single photon at 1560 nm, which is coupled into detector D4.

In the experimental setup shown in Fig. 2(b), the 140-fs pulsed laser at 780 nm (Chameleon, Coherent) is divided into two beams. One beam is frequency-doubled into 390 nm in an LBO crystal; the other serves as the pump laser for up-converting a photon from 1560 nm to 520 nm. The femtosecond laser at 390 nm is also divided and focused to pump BBO1 and BBO2 individually, with the same waist radii of 30 μm. Notably, BBO1 consists of two glued BBO pieces ($7 \times 7 \times 2$ mm^3, cutting angles $\theta = 30.5°$ and $\phi = 30°$) with orthogonal optical axes [56]. A 45°-polarized femtosecond pump laser at 390 nm is

incident on BBO1. Type-II nondegenerate SPDC could happen either in the first BBO piece or in the second piece. SPDC that occurs in the two glued BBO pieces will introduce walk-off. After the SWC and TWC operations [57,58], the down-converted photon pairs from the two BBO pieces are superposed to be a polarization-entangled state, i.e., $(1/\sqrt{2})(|H\rangle_{520}|V\rangle_{1560} + |V\rangle_{520}|H\rangle_{1560})$. The possible phase between $|H\rangle_{520}|V\rangle_{1560}$ and $|V\rangle_{520}|H\rangle_{1560}$ can be eliminated by introducing a Babinet compensator in the path of the 520-nm photon (see Appendix A for details). Using DMs, we filter out the pump laser and separate the photons at 1560 and 520 nm into two paths. Before coupling a single photon at 1560 nm into an entanglement-maintaining frequency transducer, we added a filter with a full width at half maximum (FWHM) of 25 nm to remove the stray light. Another filter with a FWHM of 3 nm is added for the single photon at 520 nm before it is detected.

A Sagnac interferometer is employed to achieve the polarization-entanglement-maintaining frequency transducer. The single photon at 1560 nm is up-converted to 520 nm at a PPLN crystal ($1 \times 2 \times 3$ mm^3) in the type-0 phase matching configuration, pumped by a femtosecond pulsed laser at 780 nm with a power of 850 mW. The photons at 1560 nm in the Sagnac interferometer have a focal radius of 160 μm measured by a camera (SP907-1550, Ophir Spiricon Inc.). We design the poled period (6.97 μm) of the PPLN crystal to maximize the conversion efficiency. Moreover, the crystal is maintained at the optimal phase-matching temperature of 135 °C. With the help of the PBS and a HWP in the Sagnac interferometer, the horizontally and vertically polarized input photons at 1560 nm pass through the PPLN crystal from the opposite directions, and are up-converted to green photons at 520 nm of vertical and horizontal polarizations, respectively. The entangled states in the Sagnac interferometer experience evolutions as follows:

$$\text{clockwise} \circlearrowright: \quad |H\rangle_{1560} \xrightarrow{\text{HWP}} |V\rangle_{1560} \xrightarrow{\text{PPLN}} |V\rangle_{520},$$
$$\text{counterclockwise} \circlearrowleft: \quad |V\rangle_{1560} \xrightarrow{\text{PPLN}} |V\rangle_{520} \xrightarrow{\text{HWP}} |H\rangle_{520}.$$
$$(1)$$

Clearly, when the photon's frequency is up-converted, its polarization is flipped. Therefore, the original entangled state is transformed as

$$\frac{1}{\sqrt{2}}(|H\rangle_{520}|V\rangle_{1560} + |V\rangle_{520}|H\rangle_{1560})$$
$$\xrightarrow{\text{transducer}} \frac{1}{\sqrt{2}}(|H\rangle_{520}|H\rangle_{520} + |V\rangle_{520}|V\rangle_{520}). \quad (2)$$

Another horizontally polarized laser beam at 390 nm pumps the BBO2, where a photon pair with the polarization state of $|V\rangle_{520}|H\rangle_{1560}$ is generated by SPDC. After DMs, the pump laser at 390 nm is filtered out, and the

photons at 1560 and 520 nm are separated. The single photon at 1560 nm is directly coupled into the single-mode fiber, and measured by the superconducting nanowire single-photon detector (P-SPD-32S, Photon Technology Co. Ltd.). As for the photon at 520 nm, it is prepared in the polarization state of $(1/\sqrt{2})(|H\rangle_{520} + |V\rangle_{520})$, and then interferes with one of the two entangled green photons at a PBS. By moving the prism placed on a translation stage, the two photons for interference arrive at the PBS simultaneously. We postselect events that represent coincident counts measured at the two output ports of the PBS, and finally successfully generate the three-photon entanglement state at 520 nm written as

$$\frac{1}{\sqrt{2}}(|H\rangle_{520}|H\rangle_{520}|H\rangle_{520} + |V\rangle_{520}|V\rangle_{520}|V\rangle_{520}), \quad (3)$$

which is accompanied by a single photon at 1560 nm. We provide details about the postselected interference at PBS in Appendix B.

In the experiment, to obtain an entangled photon pair, we need to compensate for both the time and space walk-off between horizontally and vertically polarized photons at 1560 nm (520 nm) down-converted in the first and second crystal pieces in BBO1, respectively. After several experimental attempts, the compensation scheme is determined. For the SWC of the photon at 1560 nm, two quartz crystals ($\theta = 45°$) are added. One has a length of 20.14 mm and its optical axis is along the horizontal direction, while the other has a length of 25.48 mm and its optical axis is along the vertical direction. The TWC of the photon at 1560 nm is accomplished by introducing a quartz crystal ($\theta = 0°$) with a length of 16.59 mm and its optical axis parallel to the horizontal direction. Because of the dispersion of BBO, the compensations for photons at 1560 and 520 nm are different. For the SWC of the photon at 520 nm, we use two quartz crystals ($\theta = 45°$) with the same length of 13.37 mm and whose optical axes are along orthogonal directions, i.e., horizontal and vertical directions, respectively. The TWC of the photon at 520 nm is achieved by a quartz crystal ($\theta = 0°$) with a length of 15.75 mm whose optical axis is along the horizontal direction.

Another vital improvement is that we developed the femtosecond-laser-pumped single-photon frequency up-conversion technique. In comparison, previous related experiments were implemented in a continuous-wave domain, which is not scalable in generating multiphoton entanglement, limiting its application in optical quantum computing and information. The main challenge of using the femtosecond pump laser is to achieve the temporal alignment between the 1560-nm single photon to be up-converted and the 140-fs pump laser at 780 nm in the frequency transducer—the PPLN crystal. Here, we first block the pump laser and couple the single photon at 1560 nm into the Sagnac interferometer. At the output of

the interferometer, the single photon at 1560 nm is measured by a single-photon detector, and its arrival time is recorded by a time-digital converter with a digital resolution of up to 1 ps (Time Tagger Ultra, Swabian Instruments Inc.). Then we blocked the single photon at 1560 nm and turned on the pump laser at 780 nm. Although the PPLN crystal is not designed for parametric down-conversion of photons from 780 nm to 1560 nm, a weak signal at 1560 nm can still be generated under a strong pump. The arrival time at the detectors of photons (1560 nm) spontaneously down-converted from the pump laser is also measured and tuned to be consistent with that of the input single photon at 1560 nm by moving the delay prism in the pump laser (780 nm) path. We finely tune the position of the prism to optimize up-conversion efficiency and to obtain the brightest single photon at 520 nm.

III. RESULTS AND DICUSSIONS

Under our experimental conditions, the efficiency of degenerate two-photon pair production at 520 nm is about 0.25% with respect to the two-photon pair at 520 and 1560 nm, which can be promoted by increasing the power density of the pump laser. We measure the entangled two-photon states before and after the frequency up-conversion by quantum state tomography [59], requiring that each photon is measured in $|H\rangle$, $|V\rangle$, $(1/\sqrt{2})(|H\rangle + |V\rangle)$, $(1/\sqrt{2})(|H\rangle - |V\rangle)$, $(1/\sqrt{2})(|H\rangle + i|V\rangle)$, and $(1/\sqrt{2})(|H\rangle - i|V\rangle)$ basis. For measuring the entangled state before the frequency up-conversion, we flip the polarization of the single photon at 1560 nm to have the same polarization entanglement state as that after the frequency conversion, i.e., $(1/\sqrt{2})(|HH\rangle + |VV\rangle)$. The reconstructed density matrices are shown in Fig. 3. The fidelity of measured states before and after the frequency up-conversion are 0.893 ± 0.002 and 0.746 ± 0.011, confirming that the polarization entanglement is preserved during the frequency up-conversion. We note that a weak signal at 520 nm is generated spontaneously under the pumping of the laser at 780 nm. This background may lead to a decrease in the state fidelity after frequency up-conversion. To further promote the state fidelity, we can decrease the pump power and increase the detection efficiency to lower the impact of higher-order photon-pair events [31].

Benefiting from the advantage of using a femtosecond pulsed laser in our experiment, the entangled photon number can be scaled by interfering with one of the entangled green photons with extra green photon. We now have another photon pair in the state of $|H\rangle_{1560}|V\rangle_{520}$ generated from the BBO2 crystal. The single photon at 520 nm is prepared in the polarization direction of 45° and then interferes with one of the entangled two green photons at PBS. Heralded by the single photon at 1560 nm, we postselect the coincidence at the two output ports of the PBS, together
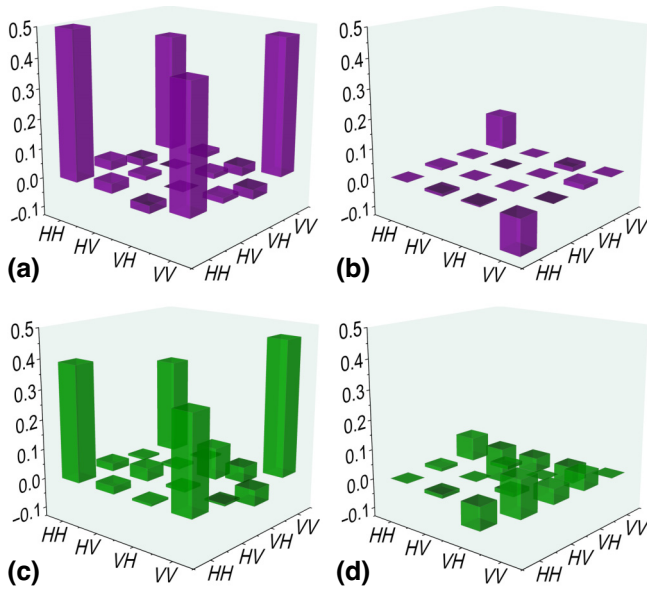
FIG. 3. Reconstructed density matrix of two-photon entangled state. (a),(b) The measured real and imaginary parts of the density matrix of the generated quantum state, whose target state is $(1/\sqrt{2})(|H\rangle_{520}|H\rangle_{1560} + |V\rangle_{520}|V\rangle_{1560})$. (c),(d) The real and imaginary parts of the density matrix of the quantum state, with the target state of $(1/\sqrt{2})(|H\rangle_{520}|H\rangle_{520} + |V\rangle_{520}|V\rangle_{520})$.

with the up-converted green photon, which is proved to be a green three-photon Greenberger-Horne-Zeilinger (GHZ) state.

The prepared GHZ state is analyzed by the following measurement. The coherence of the three-photon GHZ state, a reflection of the off-diagonal element of its density matrix, is weighted by

$$C = \frac{1}{3}\sum_{k=0}^{2}(-1)^k \langle M_{k\pi/3}^{\otimes 3}\rangle, \qquad (4)$$

where $M_{k\pi/3} = \cos(k\pi/3)\sigma_x + \sin(k\pi/3)\sigma_y$, with $k = 0, 1, 2$. The expectation of observable $M_{\theta}^{\otimes 3}$ can be obtained by measuring the three photons individually in the basis of $(1/\sqrt{2})(|H\rangle \pm e^{i\theta}|V\rangle)$, where $\theta \in \{0, \pi/3, 2\pi/3\}$. We also measure the state in the $|H\rangle/|V\rangle$ basis to get the diagonal element information of the density matrix, denoted by $P = |HHH\rangle\langle HHH| + |VVV\rangle\langle VVV|$. It is proved that the fidelity of the generated state with the perfect three-photon GHZ state as shown in Eq. (3) can be calculated by

$$F = \frac{1}{2}(\langle P\rangle + \langle C\rangle), \qquad (5)$$

where F represents the state fidelity [31,60].

In Fig. 4, we show the measured expectation values of observables $M_{\theta}^{\otimes 3}$ and P for the three-photon state, which are collected in a time duration of one hour. The errors are
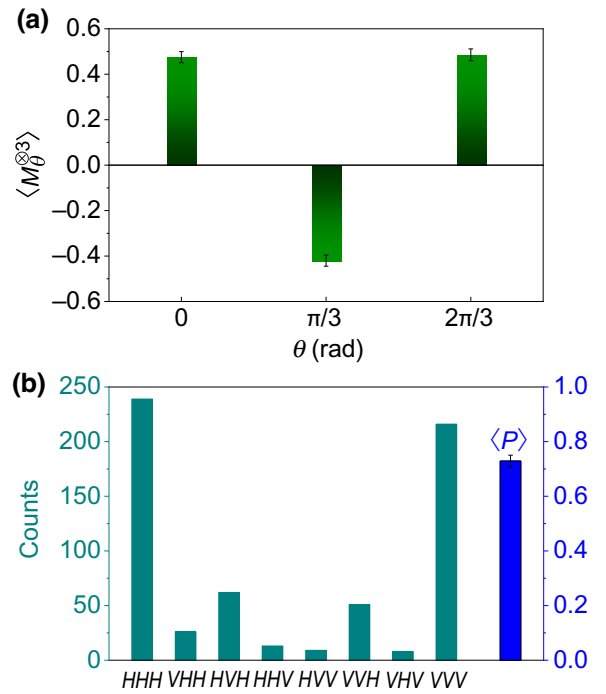

FIG. 4. Experimental results of green three-photon polarization entanglement. (a) Expectation values of $\langle M_{k\pi/3}^{\otimes 3}\rangle$ measured in the basis of $(1/\sqrt{2})(|H\rangle \pm e^{ik\pi/3}|V\rangle)$. (b) Coincidence counts when measuring the three photons in $|H/V\rangle$ basis. The calculated $\langle P\rangle$ is shown on the right.

estimated under the assumption that the photon statistics follow a Poisson distribution. From the measured results, the state fidelity we calculated is 0.595 ± 0.023. To estimate the entanglement of the prepared state, we specify the entanglement witness as $W = \alpha I + |\psi\rangle\langle\psi|$, where I is an identity matrix, $|\psi\rangle$ is the desired entanglement state as shown in Eq. (3), and α is 0.5 for the GHZ states [60,61]. It can be found that the entanglement witness is related to the state fidelity by $\langle W\rangle = 0.5 + F$. To signal the entanglement, the expectation value of W should be negative; equivalently, the state fidelity of the GHZ state must exceed 0.5. The fidelity we measured for the three-photon GHZ state exceeds the entanglement threshold 0.5 by 4.13 standard deviations, implying the presence of genuine entanglement of the three photons.

The experimental imperfections are mainly ascribed to the limited precision of the time and space walk-off compensation and the nonunity of the frequency up-conversion. For instance, the fidelities of the original two-photon entangled states (at 1560 and 520 nm) can be further promoted by choosing the compensation quartz crystals with accurate thickness. To ensure that all single photons have the probability of being frequency up-converted, we should match the pump laser with the single photon to be converted in all degrees of freedom. In our experiment, the bandwidth of the single photon is

wider than the effective bandwidth for the frequency up-conversion process. To further increase the up-conversion efficiency, one can shape the spectra of the single photon. Otherwise, the key method to improve the up-conversion efficiency is to raise the pump power.

IV. CONCLUSIONS

We have developed a polarization-entanglement-maintaining frequency-transducer technology of a femtosecond pump and experimentally achieved two- and three-green-photon entanglement. Because of the high transmission of green photons in water, our results not only pave the way for low-loss underwater and air-to-water multiparty quantum information processes [22,24], but also provide an opportunity to address the issues of heat dissipation for future quantum machines by placing them in an underwater environment on the seabed. Furthermore, the frequency-transducer technology of a femtosecond pump can be used to realize the polarization-entanglement-maintaining up-conversion with ultrathin nonlinear materials [62,63], and the generated multiphoton entangled source with short wavelength may have applications in quantum metrology [64], including supperresolving phase measurement [39].

APPENDIX A: COMPENSATION OF THE PHASE IN ENTANGLED STATES

There could be an arbitrary phase ϕ between the terms $|H\rangle_{520}|V\rangle_{1560}$ and $|V\rangle_{520}|H\rangle_{1560}$, in which case the state on the left of the arrow in Eq. (2) becomes

$$\frac{1}{\sqrt{2}}(|H\rangle_{520}|V\rangle_{1560} + e^{i\phi}|V\rangle_{520}|H\rangle_{1560}). \quad (A1)$$

To prepare the desired green-photon Bell state shown on the right of the arrow in Eq. (2), we eliminate the phase in Eq. (A1) by using a Babinet compensator, which introduces a variable phase between the horizontally and vertically polarized components for a single photon.

Rephrasing the state in Eq. (A1) in basis vectors of $|A\rangle$ and $|D\rangle$, we get

$$\frac{1}{2\sqrt{2}}[(1 + e^{i\phi})|D\rangle_{520}|D\rangle_{1560} - (1 - e^{i\phi})|D\rangle_{520}|A\rangle_{1560}$$
$$+ (1 - e^{i\phi})|A\rangle_{520}|D\rangle_{1560} - (1 + e^{i\phi})|A\rangle_{520}|A\rangle_{1560}], \quad (A2)$$

where $|A\rangle = (1/\sqrt{2})(|H\rangle + |V\rangle)$ and $|D\rangle = (1/\sqrt{2})(|H\rangle - |V\rangle)$. If we project the state in Eq. (A2) onto $|D\rangle_{520}|A\rangle_{1560}$ or $|A\rangle_{520}|D\rangle_{1560}$, the projection probability P is associated with the phase ϕ via $P = \frac{1}{4}(1 - \cos\phi)$. When $\phi = 0$, the probability of projecting onto state $|D\rangle_{520}|A\rangle_{1560}$ or $|A\rangle_{520}|D\rangle_{1560}$ vanishes. In the experiment, we project the two photons onto the $|D\rangle$ and $|A\rangle$ basis, respectively, and adjust the Babinet compensator to get the minimum twofold coincidence, and then the unknown and arbitrary phase is eliminated. The phase that could appear between the two terms in Eq. (3) is also eliminated in the same way.

APPENDIX B: ENTANGLING PHOTONS BY POSTSELECTED INTERFERENCE

After the frequency transducer, the two entangled photons of 520 nm in paths A and B are in the state of

$$\frac{1}{\sqrt{2}}(|H\rangle_{520}^A|H\rangle_{520}^B + |V\rangle_{520}^A|V\rangle_{520}^B). \quad (B1)$$

As shown in Fig. 2, to entangle the Bell state with the heralded single photon of diagonal polarization in path C, we couple the photons in paths B and C into the two ports of a PBS. Because the PBS transmits horizontally polarized photons and reflects vertically polarized photons, the PBS transforms the input state as

$$\frac{1}{2}(|H\rangle_{520}^A|H\rangle_{520}^B + |V\rangle_{520}^A|V\rangle_{520}^B) \otimes (|H\rangle_{520}^C + |V\rangle_{520}^C)$$
$$\xrightarrow{\text{PBS}} \frac{1}{2}(|H\rangle_{520}^A|H\rangle_{520}^{B'} + |V\rangle_{520}^A|V\rangle_{520}^{C'}) \otimes (|H\rangle_{520}^{C'} + |V\rangle_{520}^{B'}). \quad (B2)$$

We postselected the events that cause coincidence counts of detectors in all the paths A, B', and C'; then the state becomes

$$\frac{1}{\sqrt{2}}(|H\rangle_{520}^A|H\rangle_{520}^{B'}|H\rangle_{520}^{C'} + |V\rangle_{520}^A|V\rangle_{520}^{B'}|V\rangle_{520}^{C'}), \quad (B3)$$

which is a three-photon GHZ state that is the same as Eq. (3).

[1] A. Einstein, B. Podolsky, and N. Rosen, Can quantum-mechanical description of physical reality be considered complete? Phys. Rev. **47,** 777 (1935).

[2] J. S. Bell, On the Einstein Podolsky Rosen paradox, Phys. Physique Fizika **1,** 195 (1964).

[3] D. M. Greenberger, M. A. Horne, and A. Zeilinger, in *Bell's Theorem, Quantum Theory and Conceptions of the Universe* (Springer, Dordrecht, 1989), p. 69.

[4] C. H. Bennett, Quantum information and computation, Phys. Today **48,** 24 (1995).

[5] A. K. Ekert and R. Jozsa, Quantum algorithms: Entanglement-enhanced information processing, Philos. Trans. Royal Soc. London Ser. A **356,** 1769 (1998).

[6] P. G. Kwiat, K. Mattle, H. Weinfurter, A. Zeilinger, A. V. Sergienko, and Y. Shih, New High-Intensity Source of Polarization-Entangled Photon Pairs, Phys. Rev. Lett. **75,** 4337 (1995).

[7] A. Mair, A. Vaziri, G. Weihs, and A. Zeilinger, Entanglement of the orbital angular momentum states of photons, Nature **412,** 313 (2001).

[8] R. Fickler, G. Campbell, B. Buchler, P. K. Lam, and A. Zeilinger, Quantum entanglement of angular momentum states with quantum numbers up to 10,010, Proc. Nat. Acad. Sci. U.S.A **113,** 13642 (2016).

[9] D. Bouwmeester, J.-W. Pan, K. Mattle, M. Eibl, H. Weinfurter, and A. Zeilinger, Experimental quantum teleportation, Nature **390,** 575 (1997).

[10] M. Murao, D. Jonathan, M. Plenio, and V. Vedral, Quantum telecloning and multiparticle entanglement, Phys. Rev. A **59,** 156 (1999).

[11] X.-L. Wang, X.-D. Cai, Z.-E. Su, M.-C. Chen, D. Wu, L. Li, N.-L. Liu, C.-Y. Lu, and J.-W. Pan, Quantum teleportation of multiple degrees of freedom of a single photon, Nature **518,** 516 (2015).

[12] J.-G. Ren *et al.*, Ground-to-satellite quantum teleportation, Nature **549,** 70 (2017).

[13] S. J. Freedman and J. F. Clauser, Experimental Test of Local Hidden-Variable Theories, Phys. Rev. Lett. **28,** 938 (1972).

[14] J.-W. Pan, D. Bouwmeester, M. Daniell, H. Weinfurter, and A. Zeilinger, Experimental test of quantum nonlocality in three-photon Greenberger-Horne-Zeilinger entanglement, Nature **403,** 515 (2000).

[15] B. Hensen, H. Bernien, A. E. Dréau, A. Reiserer, N. Kalb, M. S. Blok, J. Ruitenberg, R. F. L. Vermeulen, R. N. Schouten, C. Abellán, W. Amaya, V. Pruneri, M. W. Mitchell, M. Markham, D. J. Twitchen, D. Elkouss, S. Wehner, T. H. Taminiau, and R. Hanson, Loophole-free Bell inequality violation using electron spins separated by 1.3 kilometres, Nature **526,** 682 (2015).

[16] X.-S. Ma, T. Herbst, T. Scheidl, D. Wang, S. Kropatschek, W. Naylor, B. Wittmann, A. Mech, J. Kofler, E. Anisimova, V. Makarov, T. Jennewein, R. Ursin, and A. Zeilinger, Quantum teleportation over 143 kilometres using active feed-forward, Nature **489,** 269 (2012).

[17] J. Yin *et al.*, Satellite-based entanglement distribution over 1200 kilometers, Science **356,** 1140 (2017).

[18] J. Yin *et al.*, Entanglement-based secure quantum cryptography over 1,120 kilometers, Nature **582,** 501 (2020).

[19] H.-Y. Liu, X.-H. Tian, C. Gu, P. Fan, X. Ni, R. Yang, J.-N. Zhang, M. Hu, J. Guo, X. Cao, X. Hu, G. Zhao, Y.-Q. Lu, Y.-X. Gong, Z. Xie, and S.-N. Zhu, Optical-Relayed Entanglement Distribution Using Drones as Mobile Nodes, Phys. Rev. Lett. **126,** 020503 (2021).

[20] S.-K. Liao *et al.*, Satellite-Relayed Intercontinental Quantum Network, Phys. Rev. Lett. **120,** 030501 (2018).

[21] Y.-A. Chen *et al.*, An integrated space-to-ground quantum communication network over 4,600 kilometres, Nature **589,** 214 (2021).

[22] C.-Q. Hu, Z.-Q. Yan, J. Gao, Z.-Q. Jiao, Z.-M. Li, W.-G. Shen, Y. Chen, R.-J. Ren, L.-F. Qiao, A.-L. Yang, H. Tang, and X.-M. Jin, Transmission of photonic polarization states through 55-m water: Towards air-to-sea quantum communication, Photon. Res. **7,** A40 (2019).

[23] L. Ji, J. Gao, A.-L. Yang, Z. Feng, X.-F. Lin, Z.-G. Li, and X.-M. Jin, Towards quantum communications in free-space seawater, Opt. Express **25,** 19795 (2017).

[24] F. Bouchard, A. Sit, F. Hufnagel, A. Abbas, Y. Zhang, K. Heshami, R. Fickler, C. Marquardt, G. Leuchs, R. w. Boyd, and E. Karimi, Quantum cryptography with twisted photons through an outdoor underwater channel, Opt. Express **26,** 22563 (2018).

[25] R. C. Smith and K. S. Baker, Optical properties of the clearest natural waters (200–800 nm), Appl. Opt. **20,** 177 (1981).

[26] R. Deng, Y. He, Y. Qin, Q. Chen, and L. Chen, Measuring pure water absorption coefficient in the near-infrared spectrum (900–2500 nm), Nat. Remote. Sens. Bull. **16,** 192 (2012).

[27] G. Schirripa Spagnolo, L. Cozzella, and F. Leccese, Underwater optical wireless communications: Overview, Sensors **20,** 2261 (2020).

[28] C.-Y. Lu, X.-Q. Zhou, O. Gühne, W.-B. Gao, J. Zhang, Z.-S. Yuan, A. Goebel, T. Yang, and J.-W. Pan, Experimental entanglement of six photons in graph states, Nat. Phys. **3,** 91 (2007).

[29] X.-C. Yao, T.-X. Wang, P. Xu, H. Lu, G.-S. Pan, X.-H. Bao, C.-Z. Peng, C.-Y. Lu, Y.-A. Chen, and J.-W. Pan, Observation of eight-photon entanglement, Nat. Photonics **6,** 225 (2012).

[30] C. Zhang, Y.-F. Huang, Z. Wang, B.-H. Liu, C.-F. Li, and G.-C. Guo, Experimental Greenberger-Horne-Zeilinger-Type Six-Photon Quantum Nonlocality, Phys. Rev. Lett. **115,** 260402 (2015).

[31] X.-L. Wang, L.-K. Chen, W. Li, H.-L. Huang, C. Liu, C. Chen, Y.-H. Luo, Z.-E. Su, D. Wu, Z.-D. Li, H. Lu, Y. Hu, X. Jiang, C.-Z. Peng, L. Li, N.-L. Liu, Y.-A. Chen, C.-Y. Lu, and J.-W. Pan, Experimental Ten-Photon Entanglement, Phys. Rev. Lett. **117,** 210502 (2016).

[32] H.-S. Zhong, Y. Li, W. Li, L.-C. Peng, Z.-E. Su, Y. Hu, Y.-M. He, X. Ding, W. Zhang, H. Li, L. Zhang, Z. Wang, L. You, X.-L. Wang, X. Jiang, L. Li, Y.-A. Chen, N.-L. Liu, C.-Y. Lu, and J.-W. Pan, 12-Photon Entanglement and Scalable Scattershot Boson Sampling with Optimal Entangled-Photon Pairs from Parametric Down-Conversion, Phys. Rev. Lett. **121,** 250505 (2018).

[33] V. G. Dmitriev, G. G. Gurzadyan, and D. N. Nikogosyan, *Handbook of Nonlinear Optical Crystals* (Springer, Berlin, 2013), Vol. 64.

[34] P. Kumar, Quantum frequency conversion, Opt. Lett. **15,** 1476 (1990).

[35] M. G. Raymer and K. Srinivasan, Manipulating the color and shape of single photons, Phys. Today **65**, 32 (2012).

[36] O. Kuzucu, F. N. C. Wong, S. Kurimura, and S. Tovstonog, Time-resolved single-photon detection by femtosecond upconversion, Opt. Lett. **33**, 2257 (2008).

[37] C. E. Vollmer, C. Baune, A. Samblowski, T. Eberle, V. Händchen, J. Fiurášek, and R. Schnabel, Quantum Up-Conversion of Squeezed Vacuum States from 1550 to 532 nm, Phys. Rev. Lett. **112**, 073602 (2014).

[38] Z.-Y. Zhou, S.-L. Liu, Y. Li, D.-S. Ding, W. Zhang, S. Shi, M.-X. Dong, B.-S. Shi, and G.-C. Guo, Orbital Angular Momentum-Entanglement Frequency Transducer, Phys. Rev. Lett. **117**, 103601 (2016).

[39] Z.-Y. Zhou, S.-L. Liu, S.-K. Liu, Y.-H. Li, D.-S. Ding, G.-C. Guo, and B.-S. Shi, Superresolving phase measurement with short-wavelength NOON states by quantum frequency up-conversion, Phys. Rev. Appl. **7**, 064025 (2017).

[40] S. Liu, C. Yang, Z. Xu, S. Liu, Y. Li, Y. Li, Z. Zhou, G. Guo, and B. Shi, High-dimensional quantum frequency converter, Phys. Rev. A **101**, 012339 (2020).

[41] R. Tyumenev, J. Hammer, N. Y. Joly, P. S. J. Russell, and D. Novoa, Tunable and state-preserving frequency conversion of single photons in hydrogen, Science **376**, 621 (2022).

[42] S. Tanzilli, W. Tittel, M. Halder, O. Alibart, P. Baldi, N. Gisin, and H. Zbinden, A photonic quantum information interface, Nature **437**, 116 (2005).

[43] N. Lauk, N. Sinclair, S. Barzanjeh, J. P. Covey, M. Saffman, M. Spiropulu, and C. Simon, Perspectives on quantum transduction, Quantum Sci. Technol. **5**, 020501 (2020).

[44] M. T. Rakher, L. Ma, O. Slattery, X. Tang, and K. Srinivasan, Quantum transduction of telecommunications-band single photons from a quantum dot by frequency upconversion, Nat. Photonics **4**, 786 (2010).

[45] S.-M. Li, L.-J. Kong, Z.-C. Ren, Y. Li, C. Tu, and H.-T. Wang, Managing orbital angular momentum in second-harmonic generation, Phys. Rev. A **88**, 035801 (2013).

[46] Y.-X. Yang, B.-W. Dong, Z.-C. Ren, H. Li, Y.-C. Lou, Z.-M. Cheng, Z.-F. Liu, J. Ding, X.-L. Wang, and H.-T. Wang, Nonlinear manipulation of orbital angular momentum spectra with second- and third-harmonic generation in a quasi-periodically poled crystal, Appl. Phys. Lett. **121**, 032202 (2022).

[47] X. Qiu, H. Guo, and L. Chen, Remote transport of high-dimensional orbital angular momentum states and ghost images via spatial-mode-engineered frequency conversion, Nat. Commun. **14**, 8244 (2023).

[48] B. Sephton, A. Vallés, I. Nape, M. A. Cox, F. Steinlechner, T. Konrad, J. P. Torres, F. S. Roux, and A. Forbes, Quantum transport of high-dimensional spatial information with a nonlinear detector, Nat. Commun. **14**, 8243 (2023).

[49] J.-W. Pan, Z.-B. Chen, C.-Y. Lu, H. Weinfurter, A. Zeilinger, and M. Zukowski, Multiphoton entanglement and interferometry, Rev. Mod. Phys. **84**, 777 (2012).

[50] J. Bao *et al.*, Very-large-scale integrated quantum graph photonics, Nat. Photonics **17**, 573 (2023).

[51] R. Valivarthi, M. G. Puigibert, Q. Zhou, G. H. Aguilar, V. B. Verma, F. Marsili, M. D. Shaw, S. W. Nam, D. Oblak, and W. Tittel, Quantum teleportation across a metropolitan fibre network, Nat. Photonics **10**, 676 (2016).

[52] Q.-C. Sun, Y.-L. Mao, S.-J. Chen, W. Zhang, Y.-F. Jiang, Y.-B. Zhang, W.-J. Zhang, S. Miki, T. Yamashita, H. Terai, X. Jiang, T.-Y. Chen, L.-X. You, X.-F. Chen, Z. Wang, J.-Y. Fan, Q. Zhang, and J.-W. Pan, Quantum teleportation with independent sources and prior entanglement distribution over a network, Nat. Photonics **10**, 671 (2016).

[53] Z.-C. Ren, Y.-C. Lou, Z.-M. Cheng, L. Fan, J. Ding, X.-L. Wang, and H.-T. Wang, Optical frequency conversion of light with maintaining polarization and orbital angular momentum, Opt. Lett. **46**, 2300 (2021).

[54] Y.-C. Lou, Z.-M. Cheng, Z.-H. Liu, Y.-X. Yang, Z.-C. Ren, J. Ding, X.-L. Wang, and H.-T. Wang, Third-harmonic generation of spatially structured light in a quasi-periodically poled crystal, Optica **9**, 183 (2022).

[55] S. Ramelow, A. Fedrizzi, A. Poppe, N. K. Langford, and A. Zeilinger, Polarization-entanglement-conserving frequency conversion of photons, Phys. Rev. A **85**, 013845 (2012).

[56] P. G. Kwiat, E. Waks, A. G. White, I. Appelbaum, and P. H. Eberhard, Ultrabright source of polarization-entangled photons, Phys. Rev. A **60**, R773 (1999).

[57] Y.-H. Kim, S. P. Kulik, and Y. Shih, Bell-state preparation using pulsed nondegenerate two-photon entanglement, Phys. Rev. A **63**, 060301 (2001).

[58] Y.-H. Kim, S. P. Kulik, and Y. Shih, High-intensity pulsed source of space-time and polarization double-entangled photon pairs, Phys. Rev. A **62**, 011802 (2000).

[59] D. F. V. James, P. G. Kwiat, W. J. Munro, and A. G. White, Measurement of qubits, Phys. Rev. A **64**, 052312 (2001).

[60] M. Bourennane, M. Eibl, C. Kurtsiefer, S. Gaertner, H. Weinfurter, O. Gühne, P. Hyllus, D. Bruß, M. Lewenstein, and A. Sanpera, Experimental Detection of Multipartite Entanglement Using Witness Operators, Phys. Rev. Lett. **92**, 087902 (2004).

[61] O. Gühne, C.-Y. Lu, W.-B. Gao, and J.-W. Pan, Toolbox for entanglement detection and fidelity estimation, Phys. Rev. A **76**, 030305 (2007).

[62] I. Abdelwahab, B. Tilmann, Y. Wu, D. Giovanni, I. Verzhbitskiy, M. Zhu, R. Berté, F. Xuan, L. d. S. Menezes, G. Eda, T. C. Sum, S. Y. Quek, S. A. Maier, and K. P. Loh, Giant second-harmonic generation in ferroelectric NbOI$_2$, Nat. Photonics **16**, 644 (2022).

[63] R. Camacho-Morales, D. Rocco, L. Xu, V. F. Gili, N. Dimitrov, L. Stoyanov, Z. Ma, A. Komar, M. Lysevych, F. Karouta, A. Dreischuh, H. H. Tan, G. Leo, C. D. Angelis, C. Jagadish, A. E. Miroshnichenko, M. Rahmani, and D. N. Neshev, Infrared upconversion imaging in nonlinear metasurfaces, Adv. Photonics **3**, 036002 (2021).

[64] V. Giovannetti, S. Lloyd, and L. Maccone, Advances in quantum metrology, Nat. Photonics **5**, 222 (2011).